Elevated dust depositions in West Asia linked to ocean–atmosphere shifts during North Atlantic cold events

Reza Safaierad[a], Mahyar Mohtadi[b,1], Bernd Zolitschka[c], Yusuke Yokoyama[d,e], Christoph Vogt[f], and Enno Schefuß[b]

[a]Department of Physical Geography, University of Tehran, 14155-6465 Tehran, Iran; [b]MARUM-Center for Marine Environmental Sciences, University of Bremen, 28359 Bremen, Germany; [c]Institute of Geography (GEOPOLAR), University of Bremen, 28359 Bremen, Germany; [d]Atmosphere and Ocean Research Institute, University of Tokyo, 113-0033 Tokyo, Japan; [e]Department of Earth and Planetary Sciences, University of Tokyo, 113-0033 Tokyo, Japan; and [f]Faculty of Geosciences, University of Bremen, 28359 Bremen, Germany

Edited by Yves Balkanski, Laboratoire des Sciences du Climat et de l'Environnement, Gif sur Yvette Cedex, France, and accepted by Editorial Board Member Jean Jouzel June 17, 2020 (received for review March 3, 2020)

Rapid North Atlantic cooling events during the last deglaciation caused atmospheric reorganizations on global and regional scales. Their impact on Asian climate has been investigated for monsoonal domains, but remains largely unknown in westerly wind-dominated semiarid regions. Here we generate a dust record from southeastern Iran spanning the period 19 to 7 cal. ka B.P. We find a direct link between frequent occurrences of dust plumes originating from the Arabian Peninsula and North Africa and rapid southward shifts of the westerlies associated with changes of the winter stationary waves during Heinrich Stadial 1, the Younger Dryas, the Preboreal Oscillation, and the 8.2-ka event. Dust input rises and falls abruptly at the transitions into and out of these cooling events, which we attribute to changes in the ocean circulation strength that are modulated by the North Atlantic winter sea-ice cover. Our findings reveal that waxing and waning of North American ice sheets have a stronger influence than those of European ice sheets on the winter climate over West Asia.

atmospheric dust | North Atlantic cooling | Northern Hemisphere westerlies | sea ice | West Asia

The last deglaciation is marked by rapid climate variations between ~19 and 11 cal. ka B.P. Instability of continental ice sheets and marine sea ice combined with periodic and massive iceberg surges into the North Atlantic Ocean (Heinrich events) are thought to have substantially impacted ocean–atmosphere interactions and changed the global atmospheric circulation. Proxy-based reconstructions (1, 2) and model simulations (3–5) suggest that freshwater discharge into the North Atlantic Ocean reduced northward heat transport by the Atlantic meridional overturning circulation (AMOC), which in turn translated into quasi-global climate changes during Heinrich Stadial 1 (HS1) and the Younger Dryas (YD).

The last deglaciation has been extensively studied for understanding the impact of North Atlantic cooling events on regional climate conditions. However, their impact on complex climate dynamics of West Asia, which are influenced by the Indian summer monsoon (ISM), the Northern Hemisphere westerlies (NHWs), and the Siberian High, is poorly understood (*SI Appendix*, Fig. S2). Previous studies suggest a teleconnection between North Atlantic cooling and weakening of ISM intensity (4, 6–9). However, the evidence for this teleconnection differs between marine sediments and speleothems such that the transitions into and out of stadials are abrupt in the former (7, 9, 10) but gradual in the latter (8).

To date, there are no high-resolution, well-dated terrestrial records from westerly-dominated, semiarid to arid regions in West Asia spanning the entire last deglaciation, and thus the impact of North Atlantic cold spells on this region is largely unknown. However, the existence of large subtropical deserts in and around West Asia, capable of releasing huge amounts of dust particles into the atmosphere during dry climate intervals, substantially increases the potential of West Asian sedimentary sequences to capture fingerprints of past changes in atmospheric circulation systems.

In this study, we report on multiproxy records including grain-size analysis, elemental and mineralogical compositions, and total organic matter content of a sediment core retrieved from Konar Sandal peat bog (KSB), southeastern (SE) Iran, spanning the entire last deglaciation and the Early Holocene (19 to 7 cal. ka B.P.). Our site, located near the world's largest dust sources, has a great potential to record the history of dust activities and their climate drivers. We compare our terrestrial sediment data with those from speleothems and marine sediment records in West Asia. Furthermore, we place the KSB dust record into a global context to explore the driving mechanisms of past dust activities and atmospheric circulation changes in the Northern Hemisphere.

Significance

North Atlantic cold events in the past have been shown to cause large-scale atmospheric reorganizations. Results of our dust record from southeastern Iran, which is highly susceptible to capture dust storms from North Africa and the Arabian Peninsula—the largest dust source on Earth—show a direct link between North Atlantic cooling and enhanced eastward dust transport from the Arabian Peninsula and North Africa. This finding suggests that climate conditions over western Asia during these cold events were controlled by a southward shift in the winter position of the Northern Hemisphere westerlies and more susceptible to variations in the North American winter ice cover.

Author contributions: R.S. and M.M. designed research; R.S. performed research; M.M., B.Z., Y.Y., C.V., and E.S. contributed new reagents/analytic tools; R.S., B.Z., Y.Y., and C.V. analyzed data; R.S. and M.M. wrote the paper; and R.S., M.M., B.Z., Y.Y., C.V., and E.S. discussed and interpreted the results.

The authors declare no competing interest.

This article is a PNAS Direct Submission. Y.B. is a guest editor invited by the Editorial Board.

Data deposition: All of the data that support the findings of this paper have been deposited in PANGAEA at https://doi.pangaea.de/10.1594/PANGAEA.918548.

[1]To whom correspondence may be addressed. Email: mmohtadi@marum.de.

This article contains supporting information online at https://www.pnas.org/lookup/suppl/doi:10.1073/pnas.2004071117/-/DCSupplemental.

First published July 20, 2020.

Results and Discussion

Dust Deposition in Southeastern Iran during the Last Deglaciation and the Early Holocene. Downcore variations of all lithogenic elements (Ti, Al, Si, Zr, K) in our archive (Fig. 1) indicate abrupt and large changes. Increased abundances of lithogenic elements for the periods 18 to 16.5, 15.1 to 14.6, 12.7 to 11.8, 11.2 to 11, and 8.4 to 7.8 cal. ka B.P. correspond to North Atlantic climate cold spells, i.e., HS1a and HS1c, YD, Preboreal oscillation (PBO), and the 8.2-ka event, respectively. In contrast, lithogenic abundances are low before HS1, between HS1a and HS1c (during HS1b), and during Bølling–Allerød (14.6 to 12.7 cal. ka B.P.) and the Early Holocene (11 to 8.4 cal. ka B.P.).

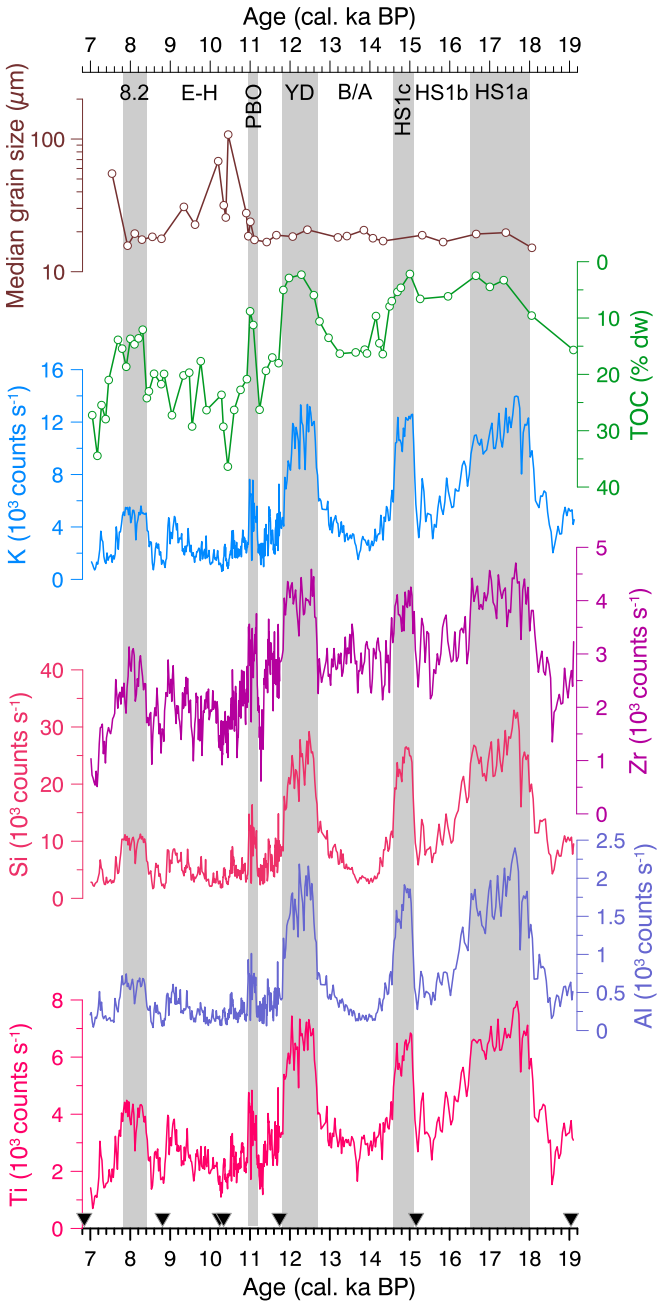

Fig. 1. Downcore element abundances for immobile (Ti, Al, Si, Zr) and mobile (K) elements along with TOC (with inverted *y* axis) and median grain size (logarithmic scale). Gray bands mark peaks of dust input. B/A, Bølling–Allerød interstadial; E-H, Early Holocene; HS1, Heinrich Stadial 1; PBO, Preboreal oscillation; YD, Younger Dryas stadial; and 8.2, the 8.2-ka event. Black triangles at the bottom indicate the position of ^{14}C age controls for KSB.

Variations in intensity of lithogenic elements are inversely correlated with total organic carbon (TOC) content of the KSB sediment core (Fig. 1), documenting that one is diluted by the other. Understanding the origin of lithogenic sediments can help to determine their controlling factor. In general, lithogenic sediments are either of local origin and transported by surface runoff or of remote, aeolian origin. Paleoclimate records from western Asia indicate dry and/or dusty climate conditions during North Atlantic cold spells in SE Iran (11), the Arabian Sea (6, 7, 10), and North Oman (12), whereas wet climatic conditions and fluvial activity dominated in SE Iran during the Early Holocene (11, 13, 14). Thus, the prevalence of dry climatic conditions as well as the lack of major riverine input into KSB does not support runoff activity to be the primary factor in transporting lithogenic material to the site during North Atlantic cold spells.

Parallel changes of mobile (K) and immobile elements (e.g., Ti) throughout the sediment core ($R^2 = 0.97$) demonstrate the lack of postdepositional changes in the mobility of elements by groundwater activity, which in turn points to the ombrotrophic nature of the KSB record. Variations in intensity of lithogenic elements such as Ti, Al, Si, Zr, and K are in phase with changes in Fe, the most abundant element (*SI Appendix*, Fig. S5), indicating that variations of these elements are not diluted by Fe-bearing components but by a similar origin of all lithogenic elements. However, some differences between variations in Fe and Ti suggest that the Fe content might be influenced by post-sedimentary processes such as oxidation. To eliminate such impacts, we prefer downcore variations in Ti for our interpretation of lithogenic input, which is neither redox sensitive nor mobile.

During the last deglaciation, the sediment composition is uniformly composed of poorly sorted sandy mud with sand not exceeding 17% in any sample, indicating the dominance of silt-sized grains that are predominantly of aeolian origin. During the Early Holocene, grain size undergoes significant changes and varies between muddy sand, mud, and sandy mud (*SI Appendix*, Fig. S4). The presence of muddy sands corresponds to the sections with maximum TOC and minimum Ti content. This is well manifested during the Early Holocene and in particular at a depth of 353 cm (10.4 cal. ka B.P.), where the maximum sand (65%) and TOC contents (36%) of the entire record occur simultaneously (Fig. 1).

The remarkable increase in TOC content during the Early Holocene points to increased humidity in the region that has been related to a strengthening and northward advance of the ISM inferred from lacustrine sediments of Lake Hamoun and the Jazmurian Playa in SE Iran (11, 14), alluvial sediments in the South Golbaf paleolake in SE Iran (13), and speleothem records from Oman (12, 15). Hence, we infer that the sand deposited in KSB is transported either by surface runoff or by Halil River flooding generated by heavy summer rainfall (*SI Appendix*, Fig. S1*B*). More importantly, very low abundances of Ti in sections with high sand contents demonstrate that the fine-grained and Ti-rich deposits are not of local origin but from distant sources transferred through aeolian processes, in accordance with the interpretation of this element in peatlands and lakes elsewhere (16, 17). Therefore, we use downcore variations of Ti as a proxy for changes of aeolian input into KSB (Fig. 1). Increased dust input in our record during the YD and the 8.2-ka event is consistent with terrestrial records from West Asia (11, 16) and with the elevated dust input during YD and HS1 in marine records from the Arabian Sea (7, 10), implying that dust plumes have occurred on a regional scale (*SI Appendix*, Fig. S6).

The mineralogy of bulk samples from sections with high and low content of Ti-rich dust indicates that variations are associated with the presence of the mineral palygorskite (Fig. 2). The presence of palygorskite during dust intervals not only confirms

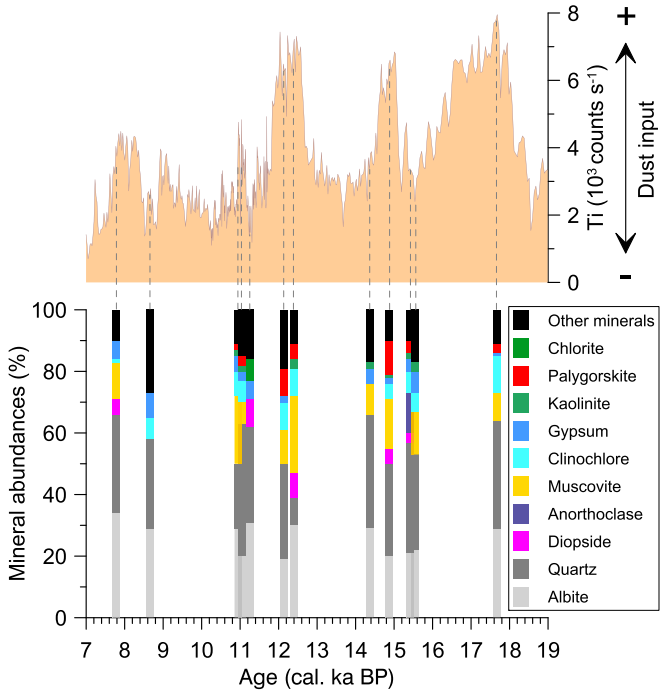

Fig. 2. Downcore variation of Ti (*Top*) and most abundant minerals determined by XRD analysis (*Bottom*).

aeolian transport of lithogenic components, but also helps to trace the provenance of dust particles. Palygorskite was found in dust minerals transported from the Arabian Peninsula and Mesopotamia to the Arabian Sea during North Atlantic cold spells (6, 18). Likewise, this mineral is one of the main constitutes of modern dust loads delivered from these sources to southwestern (SW) and western (W) Iran (19). Moreover, palygorskite is used as a tracer for dust emitted from the Sahara (20). Therefore, we infer that palygorskite deposited in our record is related to frequent dust plume occurrences on the Arabian Peninsula and in North Africa during Northern Hemisphere cold episodes.

Mechanism of West Asian Dust Plumes during North Atlantic Cold Events. To explore the driving mechanisms of dust activity in West Asia, we compare our record with the Greenland temperature (21), the AMOC strength (1), sea surface temperature (SST) and salinity in the western subtropical North Atlantic (WSTNA) (1), and dust input in Greenland ice cores (22) (Fig. 3). Variations in our dust record are consistent with changes in Greenland temperature and SST in the WSTNA during transitions into and out of stadials: Decreases (increases) in temperature are accompanied by increases (decreases) in dust input.

Fig. 3 demonstrates that dust activity in West Asia is connected to temperature changes in the North Atlantic, revealing a direct ocean–atmosphere linkage. It is generally accepted that the millennial- and centennial-scale cold events in the North Atlantic are associated with massive freshwater and iceberg discharges from continental ice sheets into the North Atlantic (23). The slowdown of AMOC induced by the influx of low-density freshwater into surface waters of the North Atlantic reduces the meridional oceanic heat transport from low to high latitudes, which eventually leads to dominance of cold temperatures across the Northern Hemisphere with maximum impact on the circum-North Atlantic realm (24).

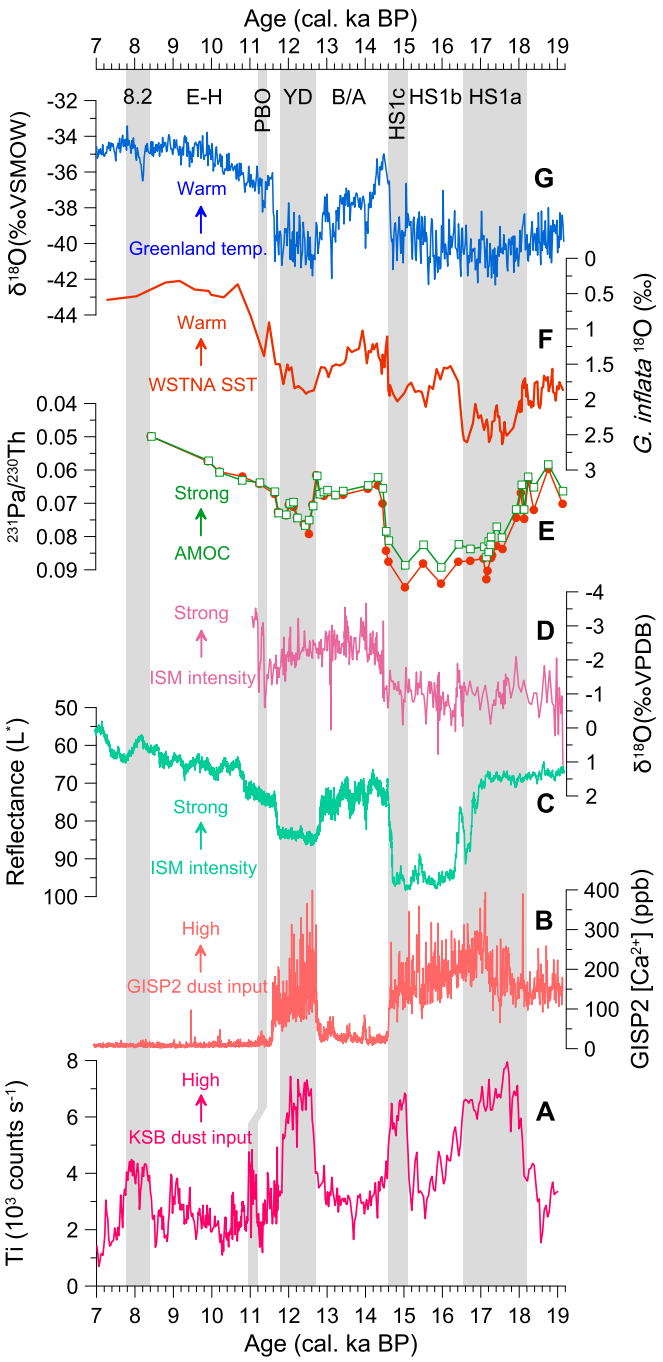

Fig. 3. (*A*, this study) Comparison of the KSB Ti record from SE Iran, representing the West Asian dust plume with paleoclimate records from Greenland ice cores, the North Atlantic Ocean and the ISM region. (*B*) Ca^{2+} concentration from Greenland Ice Sheet Project (GISP) 2 ice cores (22) as a proxy for dust input in Greenland. (*C*) Sediment color reflectance of core SO130-289KL from the northeast Arabian Sea (10) as a proxy for ISM intensity. (*D*) Speleothem $\delta^{18}O$ record from Socotra, Yemen (8) as a proxy for ISM intensity. (*E*) $^{231}Pa/^{230}Th$ ratio from the subtropical North Atlantic (1) as a proxy for the AMOC. (*F*) Subtropical North Atlantic planktic foraminifera (*Globorotalia inflata*) $\delta^{18}O$ from sediment core GGC5 (1) as a proxy for SST. (*G*) North Greenland Ice Sheet project (NGRIP) $\delta^{18}O$ values in ‰ Vienna Standard Mean Ocean Water (SMOW) on the Greenland Ice Core Chronology 2005 (GICC05) (21) as a proxy for Greenland temperature. B/A, Bølling–Allerød interstadial; E-H, Early Holocene; HS1, Heinrich Stadial 1; PBO, Preboreal oscillation; YD, Younger Dryas stadial; and 8.2, the 8.2-ka event.

The increased interhemispheric temperature contrast during these cold episodes was accompanied by global climate reorganizations (25, 26). During these episodes, the southward shift of the Intertropical Convergence Zone (ITCZ) strengthened monsoon circulations in the anomalously warm Southern Hemisphere (27, 28), but weakened the Afro-Asian northern summer monsoon system (29, 30), causing dry conditions across the monsoon domains in the Northern Hemisphere. Furthermore, the overall weakening of the Northern Hemisphere monsoon systems (31) controlled the geographical extent of other major atmospheric circulation systems in both hemispheres (26).

Large-scale climate reorganizations described above are at play with dust deposition at our site during North Atlantic cold events. According to mineralogy, dust-producing mechanisms have entrained dust particles from North Africa and the Arabian Peninsula—the World's largest dust sources—and transported them eastward toward our site, consistent with the present variations of dust input in our site showing maximum input from the Arabian Peninsula via southward-shifted westerlies in winter (32). Therefore, we deduce that HS1, YD, PBO, and the 8.2-ka event were all characterized by the flow of strong NHWs over North Africa and the Arabian Peninsula, leading to the occurrence of huge dust plumes in West Asia. This mode of explanation for increased dust input has been recently used for interpreting dust records from a loess-paleosol sequence from Hungary (33) and in lake sediments from Huguang Maar in southeast China during the Northern Hemisphere cold episodes (17), supporting the view of a global change in zonal and meridional atmospheric circulation.

A prominent feature of our dust record is the exceptionally abrupt and decadal- to multidecadal-scale (see age model in *SI Appendix*, Fig. S3) rise and fall of dust input at the onset and termination of HS1c, YD, PBO, and the 8.2-ka event, which makes it different from most (terrestrial) dust records around the world representing either gradual or less abrupt changes in dust input over the same period. The abruptness of these dust intervals points to sudden climate reorganizations induced by temperature changes over the North Atlantic and Nordic Seas at cooling and warming transitions.

Model simulations and reconstructions indicate that freshwater-forced AMOC perturbation leads to an interhemispheric heating contrast with a strong seasonality in temperature marked by maximum cooling in boreal winter (34), accompanied by an amplified seasonality in sea-ice cover with a maximum southward advance during hypercold winters (35–37). Besides the high albedo, sea ice as an insulating layer suppresses ocean heat loss to the atmosphere and thereby substantially reduces the surface air temperature over the ice-covered ocean (38). To compensate the reduced northward cross-equatorial oceanic heat transport in the Atlantic Ocean, the ITCZ and the Hadley circulation shift toward the anomalously warm Southern Hemisphere. Consequently, the modified tropical–extratropical atmospheric circulations in boreal winter involve a southward shift in the westerlies that are stronger and gustier due to steep temperature and pressure gradients between the sea-ice–covered and sea-ice–free ocean (39). Superimposed on latitudinal shifts in atmospheric circulation, freshwater hosing experiments show a change in the stationary wave trains due to the development of large cyclonic–anticyclonic anomalies over the heterogeneously cooled regions in boreal winter during intervals of weakened AMOC (4, 40). In particular, the adjustment of the atmospheric circulations involves anticyclonic circulations over the central Mediterranean Sea and the Indian Subcontinent and a cyclonic circulation over the Arabian Peninsula that gives rise to a large-amplitude stationary trough over the Red Sea (4, 40). The development of this upper-level trough reinforces the surface convergence over the Arabian Peninsula and depending on whether the advected air into the surface convergence is humid or dry, the deep trough system can result in heavy rainfall (41) or widespread dust plumes (42) in West Asia, respectively. Once strong and dry winds entrain and transport dust into the surface convergence, the upper-level jet stream carries these dust loads eastward and generates widespread dust plumes over West Asia.

Paleoclimate records from the Arabian Sea (43) and the Red Sea (44), as major sources of moisture for rainfall associated with the Red Sea trough, indicate sea surface cooling during HS1 and the YD that results in dry air advection into the surface convergence over the Arabian Peninsula. Dry air advection combined with increased aridity in the Afro-Asian monsoon domains (5, 40) favors the generation of dust plumes. Importantly, the response of stationary wave trains to the AMOC slowdown is rapid and appears within decades after the initial perturbation of the AMOC (45). These mechanisms associated with the AMOC-forced changes in the NHWs, ITCZ, and stationary waves explain the rapid onset and termination of the intervals of frequent wintertime dust plumes in West Asia during stadials, as recorded by our data. This interpretation is consistent with the abrupt increase in dust deposition over Europe (33) and East Asia (17), as well as with abrupt deglacial climate changes recorded in Lake Meerfelder Maar in Germany (46), and an abrupt increase in winter precipitation in the SW United States during stadials (47, 48), which all have been attributed to a rapid change in the NHWs during winter.

The occurrence of winter dust plumes in West Asia is therefore responsible for the increased influx of palygorskite and other Mg-bearing dust minerals from the Arabian Peninsula into the Arabian Sea during stadials (6, 49, 50). Thus, the abrupt changes registered by marine sediments of the northern Arabian Sea during stadials (7, 10) might reflect both an increase in westerly wind intensity during winter and a decrease in monsoon strength during summer. Pronounced changes in the upwelling-induced productivity in marine sediments from the northern Arabian Sea (7) also show the high sensitivity of these archives to wind changes. Instead, speleothems as archives of past hydrological variability and without sensitivity to winter wind/dust changes might better represent the ISM strength and reflect less abrupt changes of the summer monsoon at transitions into stadials and interstadials.

Unlike Europe, where the enhanced dust emissions during stadials are attributed primarily to changes in vegetation cover (51), North Africa and the Arabian Peninsula are intrinsically dry and constitute the largest dust sources in the world. Atmospheric circulations involving high-speed surface winds could drive dust mobilization and transport from such desert environments (52). The increased dust emission from these regions during stadials is thus most plausibly linked to wind speed changes associated with large-scale atmospheric reconfigurations. This notion is supported by the gradual decreasing trends in our dust record, e.g., during the YD, which mimics the pattern of dust deposition in Greenland ice cores (Fig. 3), suggesting the role of decreased wind gustiness on a global scale, as the sources of dust emissions for these regions are not the same. Nevertheless, the overall Northern Hemisphere aridity during stadials as well as sea surface cooling over the moisture sources for West Asian precipitation might have also contributed to the augmented dust emissions from the dust sources.

Generally, HS1 (ca. 18 to 14.6 cal. ka B.P.) is considered as a two- or three-step event (53–56). The early stage is thought to be associated with meltwater discharge into the North Atlantic from Eurasian and North American ice sheets as a consequence of the temperature rise at the beginning of the last deglaciation (57–59). The late stage is attributed to massive iceberg discharges from the unstable Laurentide Ice Sheet (LIS) into the North Atlantic (57, 58). HS1 is not a uniform event in our record as well and contains two dust phases (HS1a and HS1c), separated by an intervening period of declined dust input (HS1b).

The first phase (HS1a) begins at 18 cal. ka B.P. and remains relatively constant until 16.5 cal. ka B.P. and then gradually decreases. The second phase (HS1c) begins very rapidly at 15.1 cal. ka B.P. and ends suddenly with the onset of the Bølling–Allerød at 14.6 cal. ka B.P. (Fig. 3). The enhanced dust activity at the onset of HS1a is in agreement with the freshwater release from European ice sheets into the North Atlantic between 18.2 ± 0.2 and 16.7 ± 0.2 ka B.P. (59), but not with temperature and dust records of Greenland. The gradual decline of dust input in our record after 16.5 cal. ka B.P. is well matched by the termination of freshwater discharge from European ice sheets into the North Atlantic. The North Atlantic sea-ice cover must have been reduced from the WSTNA at 16.5 cal. ka B.P. and steadily receded to more northern regions, leading to a concomitant northward displacement of the NHWs. This is in line with increased humidity in northeastern (NE) Brazil at 16.5 ka B.P., attributed to a northward shift of the ITCZ (53) and a surface warming trend in the western South Atlantic between 16.5 and 15.1 cal. ka B.P., attributed to increased AMOC strength (60).

The abrupt onset of HS1c at 15.1 cal. ka B.P. is in agreement with the strongest expansion of perennial sea-ice cover in the SE Norwegian Sea over the past 90 ky (61). It is also synchronous with the destabilization and rapid thinning of the LIS (62, 63) and discharge of massive icebergs and freshwater from this giant ice mass into the North Atlantic through the Hudson Strait (58), the Gulf of Maine (62, 63), and the Gulf of Mexico (64). Furthermore, this event is well matched with a rapid SST warming in the western South Atlantic (60), elucidating the rapid response of atmospheric circulation to AMOC variability on a global scale (*SI Appendix*, Fig. S7).

Variations in our dust record suggest that North Atlantic cold events caused by discharges of freshwater and icebergs from the North American ice sheets (HS1c, YD, PBO, and the 8.2-ka event) have led to more rapid climate reorganizations in West Asia compared to those caused by European ice sheets (HS1a). This may be associated with the flow pattern of the Gulf Stream along the East Coast of North America, making it more sensitive to freshwater and iceberg discharges from this continent. As a result, freshwater and iceberg discharges from the LIS and/or Lake Agassiz appear to have profoundly reduced the strength of the AMOC and caused a widespread cooling and rapid sea-ice advance in the mid- and high-latitude North Atlantic, leading to a large meridional shift in NHWs. In contrast, freshwater and iceberg discharges from the European ice sheets have most likely caused a progressive sea-ice advance from the high- toward the midlatitude North Atlantic, which resulted in less abrupt meridional shifts in the NHWs.

Materials and Methods

A 7.63-cm-long sediment core was collected from KSB located ca. 20 km south of the city of Jiroft in Kerman Province, SE Iran and 2 km west of the 390-km-long Halil River (*SI Appendix*, Text and Fig. S1 *A* and *B*). Here we report on the section between 169 and 763 cm sediment depth, spanning the time period 19 to 6.85 cal. ka B.P. The age model is based on linear interpolation between seven radiocarbon dates (*SI Appendix*, Table S1 and Fig. S3). X-ray fluorescence (XRF)-core scanning was processed using the AVAATECH XRF core scanner at MARUM, University of Bremen. Data were scanned every 1 cm downcore across a 12-mm^2 area with a slit size of 10 mm using voltages of 50, 30, and 10 kV with 0.75, 0.75, and 0.2 mA and analyzing times of 25, 20, and 15 s, respectively. For X-ray diffraction (XRD) analysis, 12 samples each with about 1 g weight were measured on a Philips X′Pert Pro multipurpose diffractometer equipped with a Cu-tube (k′′ 1.541, 45 kV, 40 mA), a fixed divergence slit of 1/4°, a 16-sample changer, a secondary Ni-Filter, and the X′Celerator detector system. For grain-size analysis, 29 samples of 0.3 g were treated with H_2O_2 to remove organic matter. Prior to analysis with a LS 200 Laser Diffraction Particle Size Analyzer (Beckman Coulter) equipped with a variable-speed module, samples were dispersed with 20 mL of Calgon, agitated with a shaking device, transferred to the analyzing unit through a 2-mm sieve, and measured at least four times for 60 s with sonification. For organic carbon measurement, a total of 60 dried and homogenized samples were weighed into silver capsules and pretreated with 3 and 20% HCl overnight at a temperature of 80 °C to remove carbonates. Samples were analyzed with a Euro-EA Elemental Analyzer (*SI Appendix*).

Data Availability. All of the data that support the findings of this study can be found in Dataset S3 and refs. 1, 8, 10, 21, 22, and 65. All data from KSB core have been deposited in the PANGAEA data repository and are accessible at https://doi.pangaea.de/10.1594/PANGAEA.918548.

ACKNOWLEDGMENTS. We thank Sabine Stahl, Rafael Stiens, and Vera Lukies for technical support. We are grateful to Dariush Noorollahi for his assistance during fieldwork and collaboration with organic carbon measurements and to Musa Aghajani for his help during fieldwork. M.M. acknowledges support by Bundesministerium für Bildung und Forschung (BMBF) Grant 03G0864F. Y.Y. received funding from Japan Society for the Promotion of Science (JSPS) Kakenhi Grants 17H01168 and 20H00193. C.V. thanks the XRD laboratory/crystallography crew for providing perfect analysis conditions.

1. J. F. McManus, R. Francois, J.-M. Gherardi, L. D. Keigwin, S. Brown-Leger, Collapse and rapid resumption of Atlantic meridional circulation linked to deglacial climate changes. *Nature* **428**, 834–837 (2004).
2. L. C. Peterson, G. H. Haug, K. A. Hughen, U. Röhl, Rapid changes in the hydrologic cycle of the tropical Atlantic during the last glacial. *Science* **290**, 1947–1951 (2000).
3. M. Kageyama *et al*., Climatic impacts of fresh water hosing under last glacial maximum conditions: A multi-model study. *Clim. Past* **9**, 935–953 (2013).
4. M. Mohtadi *et al*., North Atlantic forcing of tropical Indian Ocean climate. *Nature* **509**, 76–80 (2014).
5. C. Marzin, N. Kallel, M. Kageyama, J.-C. Duplessy, P. Braconnot, Glacial fluctuations of the Indian monsoon and their relationship with North Atlantic climate: New data and modelling experiments. *Clim. Past* **9**, 2135–2151 (2013).
6. F. Sirocko, D. Garbe-Schönberg, A. McIntyre, B. Molfino, Teleconnections between the subtropical monsoons and high-latitude climates during the last deglaciation. *Science* **272**, 526–529 (1996).
7. A. Pourmand, F. Marcantonio, H. Schulz, Variations in productivity and eolian fluxes in the northeastern Arabian Sea during the past 110 ka. *Earth Planet. Sci. Lett.* **221**, 39–54 (2004).
8. J. D. Shakun *et al*., A high-resolution, absolute-dated deglacial speleothem record of Indian Ocean climate from Socotra Island, Yemen. *Earth Planet. Sci. Lett.* **259**, 442–456 (2007).
9. H. Schulz, U. von Rad, H. Erlenkeuser, Correlation between Arabian Sea and Greenland climate oscillations of the past 110,000 years. *Nature* **393**, 54 (1998).
10. G. Deplazes *et al*., Links between tropical rainfall and North Atlantic climate during the last glacial period. *Nat. Geosci.* **6**, 213 (2013).
11. A. Vaezi *et al*., A Late Pleistocene-Holocene multi-proxy record of climate variability in the Jazmurian playa, southeastern Iran. *Palaeogeogr. Palaeoclimatol. Palaeoecol.* **514**, 754–767 (2019).
12. D. Fleitmann *et al*., Holocene ITCZ and Indian monsoon dynamics recorded in stalagmites from Oman and Yemen (Socotra). *Quat. Sci. Rev.* **26**, 170–188 (2007).
13. R. Walker *et al*., Holocene slip-rate on the Gowk strike-slip fault and implications for the distribution of tectonic strain in eastern Iran. *Geophys. J. Int.* **181**, 221–228 (2010).
14. M. A. Hamzeh *et al*., Holocene hydrological changes in SE Iran, a key region between Indian summer monsoon and Mediterranean winter precipitation zones, as revealed from a lacustrine sequence from Lake Hamoun. *Quat. Int.* **408**, 25–39 (2016).
15. D. Fleitmann *et al*., Holocene forcing of the Indian monsoon recorded in a stalagmite from southern Oman. *Science* **300**, 1737–1739 (2003).
16. A. Sharifi *et al*., Early-Holocene greening of the Afro-Asian dust belt changed sources of mineral dust in West Asia. *Earth Planet. Sci. Lett.* **481**, 30–40 (2018).
17. G. Yancheva *et al*., Influence of the intertropical convergence zone on the East Asian monsoon. *Nature* **445**, 74–77 (2007).
18. N. Fagel, P. D. E. Debrabant, P. Menocal, B. Demoulin, Use of sedimentary clay-minerals for the reconstitution of periodic paleoclimatic variations in the Arabian Sea. *Oceanol. Acta* **15**, 125–136 (1992).
19. M. S. Najafi *et al*., Characteristics of TSP loads during the Middle East springtime dust storm (MESDS) in Western Iran. *Arab. J. Geosci.* **7**, 5367–5381 (2014).
20. D. Scheuvens, L. Schuetz, K. Kandler, M. Ebert, S. Weinbruch, Bulk composition of northern African dust and its source sediments—A compilation. *Earth Sci. Rev.* **116**, 170–194 (2013).
21. A. Svensson *et al*., A 60 000 year Greenland stratigraphic ice core chronology. *Clim. Past* **4**, 47–57 (2008).
22. P. A. Mayewski *et al*., Major features and forcing of high-latitude northern hemisphere atmospheric circulation using a 110,000-year-long glaciochemical series. *J. Geophys. Res. Oceans* **102**, 26345–26366 (1997).
23. G. C. Bond, R. Lotti, Iceberg discharges into the North Atlantic on millennial time scales during the last glaciation. *Science* **267**, 1005–1010 (1995).

24. J. T. Overpeck, L. C. Peterson, N. Kipp, J. Imbrie, D. Rind, Climate change in the circum-North Atlantic region during the last deglaciation. *Nature* **338**, 553 (1989).
25. P. U. Clark *et al*., Global climate evolution during the last deglaciation. *Proc. Natl. Acad. Sci. U.S.A.* **109**, E1134–E1142 (2012).
26. J. S. Singarayer, P. J. Valdes, W. H. G. Roberts, Ocean dominated expansion and contraction of the late Quaternary tropical rainbelt. *Sci. Rep.* **7**, 9382 (2017).
27. N. M. Stríkis *et al*., South American monsoon response to iceberg discharge in the North Atlantic. *Proc. Natl. Acad. Sci. U.S.A.* **115**, 3788–3793 (2018).
28. L. C. Kanner, S. J. Burns, H. Cheng, R. L. Edwards, High-latitude forcing of the South American summer monsoon during the last glacial. *Science* **335**, 570–573 (2012).
29. J. C. Stager, D. B. Ryves, B. M. Chase, F. S. Pausata, Catastrophic drought in the Afro-Asian monsoon region during Heinrich event 1. *Science* **331**, 1299–1302 (2011).
30. Y.-J. Wang *et al*., A high-resolution absolute-dated late Pleistocene monsoon record from Hulu Cave, China. *Science* **294**, 2345–2348 (2001).
31. M. Mohtadi, M. Prange, S. Steinke, Palaeoclimatic insights into forcing and response of monsoon rainfall. *Nature* **533**, 191–199 (2016).
32. M. H. Mahoutchi, M. Khazaie, M. Jalilian, "Identification of the dominant patterns of severe dust storms in Kerman province". *Proceedings of 3rd International Conference on New Findings of Agriculture, Natural Resources and Environment* (2017).
33. G. Újvári *et al*., Coupled European and Greenland last glacial dust activity driven by North Atlantic climate. *Proc. Natl. Acad. Sci. U.S.A.* **114**, E10632–E10638 (2017).
34. G. H. Denton, R. B. Alley, G. C. Comer, W. S. Broecker, The role of seasonality in abrupt climate change. *Quat. Sci. Rev.* **24**, 1159–1182 (2005).
35. C. Li, D. S. Battisti, D. P. Schrag, E. Tziperman, Abrupt climate shifts in Greenland due to displacements of the sea ice edge. *Geophys. Res. Lett.* **32**, L19702 (2005).
36. H. Renssen, R. Isarin, The two major warming phases of the last deglaciation at ∼14.7 and ∼11.5 ka cal BP in Europe: Climate reconstructions and AGCM experiments. *Global Planet. Change* **30**, 117–153 (2001).
37. H. Renssen, M. Lautenschlager, C. Schuurmans, The atmospheric winter circulation during the Younger Dryas stadial in the Atlantic/European sector. *Clim. Dyn.* **12**, 813–824 (1996).
38. J. E. Kutzbach, W. F. Ruddiman, H. Wright, *"Model description, external forcing, and surface boundary conditions" in Global Climates Since the Last Glacial Maximum*, H. E. Wright, Ed. *et al.* (University of Minnesota Press, 1993), pp. 12–23.
39. D. McGee, W. S. Broecker, G. Winckler, Gustiness: The driver of glacial dustiness? *Quat. Sci. Rev.* **29**, 2340–2350 (2010).
40. M. Kageyama *et al*., Glacial climate sensitivity to different states of the Atlantic meridional overturning circulation: Results from the IPSL model. *Clim. Past* **5**, 551–570 (2009).
41. U. Dayan, R. Abramski, Heavy rain in the Middle East related to unusual jet stream properties. *Bull. Am. Meteorol. Soc.* **64**, 1138–1140 (1983).
42. P. Jish Prakash, G. L. Stenchikov, S. Kalenderski, S. Osipov, H. K. Bangalath, The impact of dust storms on the Arabian Peninsula and the Red Sea. *Atmos. Chem. Phys.* **15**, 199–222 (2015).
43. J. E. Tierney, F. S. Pausata, P. Demenocal, Deglacial Indian monsoon failure and North Atlantic stadials linked by Indian Ocean surface cooling. *Nat. Geosci.* **9**, 46 (2016).
44. H. W. Arz, J. Pätzold, P. J. Müller, M. O. Moammar, Influence of Northern Hemisphere climate and global sea level rise on the restricted Red Sea marine environment during termination I. *Paleoceanography* **18**, 1053 (2003).
45. M. Vellinga, R. A. Wood, Global climatic impacts of a collapse of the Atlantic thermohaline circulation. *Clim. Change* **54**, 251–267 (2002).
46. A. Brauer, G. H. Haug, P. Dulski, D. M. Sigman, J. F. Negendank, An abrupt wind shift in western Europe at the onset of the Younger Dryas cold period. *Nat. Geosci.* **1**, 520–523 (2008).
47. Y. Asmerom, V. J. Polyak, S. J. Burns, Variable winter moisture in the southwestern United States linked to rapid glacial climate shifts. *Nat. Geosci.* **3**, 114–117 (2010).
48. D. McGee, E. Moreno-Chamarro, J Marshall, E. Galbraith, Western US lake expansions during Heinrich stadials linked to Pacific Hadley circulation. *Sci. Adv.* **4**, eaav0118 (2018).
49. G. Deplazes *et al*., Weakening and strengthening of the Indian monsoon during Heinrich events and Dansgaard-Oeschger oscillations. *Paleoceanography* **29**, 99–114 (2014).
50. F. Sirocko, H. Lange, Clay-mineral accumulation rates in the Arabian Sea during the late Quaternary. *Mar. Geol.* **97**, 105–119 (1991).
51. A. Sima *et al*., Imprint of North-Atlantic abrupt climate changes on western European loess deposits as viewed in a dust emission model. *Quat. Sci. Rev.* **28**, 2851–2866 (2009).
52. D. McGee, P. B. deMenocal, G. Winckler, J.-B. W. Stuut, L. Bradtmiller, The magnitude, timing and abruptness of changes in North African dust deposition over the last 20,000 yr. *Earth Planet. Sci. Lett.* **371**, 163–176 (2013).
53. L. M. Dupont *et al*., Two-step vegetation response to enhanced precipitation in Northeast Brazil during Heinrich event 1. *Glob. Change Biol.* **16**, 1647–1660 (2010).
54. W. Broecker, A. E. Putnam, How did the hydrologic cycle respond to the two-phase mystery interval? *Quat. Sci. Rev.* **57**, 17–25 (2012).
55. I. Bouimetarhan *et al*., Sahel megadrought during Heinrich Stadial 1: Evidence for a three-phase evolution of the low-and mid-level West African wind system. *Quat. Sci. Rev.* **58**, 66–76 (2012).
56. J. Stanford *et al*., A new concept for the paleoceanographic evolution of Heinrich event 1 in the North Atlantic. *Quat. Sci. Rev.* **30**, 1047–1066 (2011).
57. H. C. Ng *et al*., Coherent deglacial changes in western Atlantic Ocean circulation. *Nat. Commun.* **9**, 2947 (2018).
58. D. A. Hodell *et al*., Anatomy of Heinrich Layer 1 and its role in the last deglaciation. *Paleoceanography* **32**, 284–303 (2017).
59. S. Toucanne *et al*., Millennial-scale fluctuations of the European Ice Sheet at the end of the last glacial, and their potential impact on global climate. *Quat. Sci. Rev.* **123**, 113–133 (2015).
60. C. M. Chiessi *et al*., Thermal evolution of the western South Atlantic and the adjacent continent during Termination 1. *Clim. Past* **11**, 915–929 (2015).
61. U. Hoff, T. L. Rasmussen, R. Stein, M. M. Ezat, K. Fahl, Sea ice and millennial-scale climate variability in the Nordic seas 90 kyr ago to present. *Nat. Commun.* **7**, 12247 (2016).
62. P. T. Davis, P. R. Bierman, L. B. Corbett, R. C. Finkel, Cosmogenic exposure age evidence for rapid Laurentide deglaciation of the Katahdin area, west-central Maine, USA, 16 to 15 ka. *Quat. Sci. Rev.* **116**, 95–105 (2015).
63. A. J. Koester *et al*., Rapid thinning of the Laurentide ice sheet in coastal Maine, USA, during late Heinrich Stadial 1. *Quat. Sci. Rev.* **163**, 180–192 (2017).
64. C. Williams, B. P. Flower, D. W. Hastings, Seasonal Laurentide ice sheet melting during the "Mystery Interval" (17.5–14.5 ka). *Geology* **40**, 955–958 (2012).
65. R. Safaierad, M. Mohtadi, B. Zolitschka, Y. Yokoyama, C. Vogt, E. Schefuß, XRF, XRD, grainsize and total organic carbon in core Konar Sandal peat bog, SE Iran. PANGAEA, https://doi.pangaea.de/10.1594/PANGAEA.918548. Deposited 9 June 2020.